

## Modifications to the Rapid Update Cycle Land Surface Model (RUC LSM) Available in the Weather Research and Forecasting (WRF) Model

TATIANA G. SMIRNOVA

*NOAA/Earth System Research Laboratory, and Cooperative Institute for Research in  
Environmental Sciences, Boulder, Colorado*

JOHN M. BROWN AND STANLEY G. BENJAMIN

*NOAA/Earth System Research Laboratory, Boulder, Colorado*

JAYMES S. KENYON

*NOAA/Earth System Research Laboratory, and Cooperative Institute for Research in  
Environmental Sciences, Boulder, Colorado*

(Manuscript received 19 May 2015, in final form 30 November 2015)

### ABSTRACT

The land surface model (LSM) described in this manuscript was originally developed as part of the NOAA Rapid Update Cycle (RUC) model development effort; with ongoing modifications, it is now used as an option for the WRF community model. The RUC model and its WRF-based NOAA successor, the Rapid Refresh (RAP), are hourly updated and have an emphasis on short-range, near-surface forecasts including aviation-impact variables and preconvective environment. Therefore, coupling to this LSM (hereafter the RUC LSM) has been critical to provide more accurate lower boundary conditions. This paper describes changes made to the RUC LSM since earlier descriptions, including extension from six to nine levels, improved snow treatment, and new land-use data from MODIS.

The RUC LSM became operational at the NOAA/National Centers for Environmental Prediction (NCEP) as part of the RUC from 1998–2012 and as part of the RAP from 2012 through the present. The simple treatments of basic land surface processes in the RUC LSM have proven to be physically robust and capable of realistically representing the evolution of soil moisture, soil temperature, and snow in cycled models. Extension of the RAP domain to encompass all of North America and adjacent high-latitude ocean areas necessitated further development of the RUC LSM for application in the tundra permafrost regions and over Arctic sea ice. Other modifications include refinements in the snow model and a more accurate specification of albedo, roughness length, and other surface properties. These recent modifications in the RUC LSM are described and evaluated in this paper.

### 1. Introduction

The context of this work is an ongoing effort within the NOAA/Earth System Research Laboratory to improve prediction of land surface and hydrological

properties in NOAA models. The land surface model (LSM) described in this paper was originally developed to provide more accurate lower boundary conditions for the hourly updated NOAA Rapid Update Cycle (RUC) model focusing on short-range aviation and severe weather prediction (Benjamin et al. 2004a) but has now been extended to wider geographical application. These recent applications include the Weather Research and Forecasting (WRF) Model (Skamarock et al. 2008) and the NOAA hourly updated Rapid Refresh (RAP; Benjamin et al. 2016) and High-Resolution Rapid Refresh (HRRR; Smith et al. 2008) models. The goal of this study is to describe and

---

 Denotes Open Access content.

---

*Corresponding author address:* Tatiana G. Smirnova, Global Systems Division, NOAA/ESRL, 325 Broadway, Boulder, CO 80305.

E-mail: tanya.smirnova@noaa.gov

DOI: 10.1175/MWR-D-15-0198.1

TABLE 1. Modifications to the RUC LSM implemented in the WRF version 3.6 model (2014) compared to its predecessor 2000 version. Abbreviations: MODIS = Moderate Resolution Imaging Spectroradiometer; FPAR = fractional photosynthetically active radiation; IGBP = International Geosphere–Biosphere Programme; AVHRR = Advanced Very High Resolution Radiometer; LAI = leaf area index; DMSP = Defense Meteorological Satellite Program.

RUC LSM characteristics	Smirnova et al. (2000)	WRF version 3.6, 2014
Prognostic vertical levels	Soil = 6 levels (0, 5, 20, 40, 160, 300 cm), snow = 2 levels	Soil = 9 levels (0, 1, 4, 10, 30, 60, 100, 160, 300 cm), snow = 2 levels
Sea ice model	None	Heat diffusion; snow on ice
Snow model	Two-layer snow model, snow area trimming	Two-layer snow model with improvements in snow melting algorithm, snow area trimming/building
Snow melting	Single-iteration energy budget	Two-iteration energy budget
Snow albedo	Constant value (0.75)	Clear-sky maximum surface albedo of snow-covered land computed from DMSP imagery, temperature dependence
Land-use classification	USGS categories	MODIS IGBP-modified categories
Vegetation fraction, LAI	0.144° resolution AVHRR vegetation fraction, no LAI	1-km resolution MODIS FPAR/LAI data;
Surface parameters	Look-up tables for dominant category	Subgrid-scale heterogeneity, includes seasonal variations

validate the modifications to the RUC LSM that are motivated by these new applications.

A previous six-level version of a land surface soil–vegetation scheme (Smirnova et al. 1997) was incorporated into the cycled RUC model to improve its predictions of surface fluxes and atmospheric boundary layer properties by explicitly predicting soil moisture and temperature using full soil-condition cycling as part of ongoing short-range prediction and frequent data assimilation. This provided an alternative to use of climatological soil values that can result in significant errors during and after dry or rainy periods. Later, this surface model, referred to as the RUC LSM, was enhanced to include a snow model and frozen soil processes (Smirnova et al. 2000). The parameterizations in the RUC LSM describe complicated atmosphere–land surface interactions in an intentionally simplified fashion to avoid excessive sensitivity to multiple uncertain surface parameters. Nevertheless, the RUC LSM, when coupled with the hourly-assimilating RUC atmospheric model, demonstrated over years of ongoing cycling (Benjamin et al. 2004a,b; Berbery et al. 1999) that it can produce a realistic evolution of hydrologic and time-varying soil fields (i.e., soil moisture and temperature) that cannot be directly observed over large areas. This result is possible only if the soil–vegetation–snow component of the coupled model, constrained only by atmospheric boundary conditions and the specification of surface characteristics, has sufficient skill to avoid long-term drift.

To validate physical parameterizations, land surface models are customarily tested offline and forced with observed atmospheric conditions, thereby providing a controlled environment so model behavior can be assessed. A set of more recent RUC LSM modifications (Table 1) have been developed and evaluated through

such offline testing and coupled numerical weather prediction (NWP) testing, as described in this paper. International projects for intercomparison of land surface and snow parameterization schemes were essential in providing this testing environment and afforded an excellent opportunity to evaluate the RUC LSM with different land use and soil types and within a variety of climates. The RUC LSM was included in phase 2(d) of the Project for the Intercomparison of Land Surface Prediction Schemes [PILPS-2(d)], in which tested models performed 18-yr simulations of the land surface state (Schlosser et al. 1997; Slater et al. 2001; Luo et al. 2003). The RUC LSM was also tested during the Snow Models Intercomparison Project (SnowMIP and SnowMIP2), with emphasis on snow parameterizations for both grassland and forest locations (Etchevers et al. 2002, 2004; Essery et al. 2009; Rutter et al. 2009). Selected results from these offline experiments will be presented in this paper.

In 1998, the initial RUC LSM was implemented in the operational RUC at NCEP; it then became available worldwide in 2002 as an LSM option through the WRF community model (<http://wrf-model.org>; Skamarock et al. 2008). The RAP model (Benjamin et al. 2007, 2016), implemented at NCEP in May 2012 (and replacing the RUC), uses the Advanced Research WRF (ARW) dynamical core as the prognostic atmospheric model component and the RUC LSM option as its land surface component. With the RAP domain extending into the Arctic region (Fig. 1), the RUC LSM needed further development to improve an interactive coupling of the atmosphere with the underlying surface where it is ice covered.

As a first step, a simple sea ice treatment and further snow component enhancements were added to the RUC LSM. Later, vertical resolution in the soil domain was

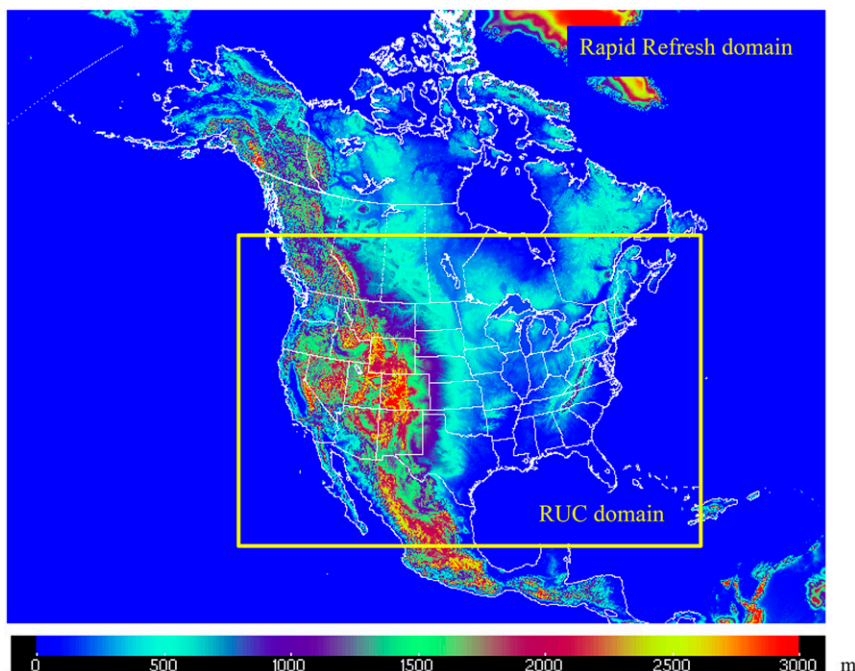


FIG. 1. Topography image (elevation in meters) of the North America RAP domain with embedded RUC domain also shown [assumed to be equal to the conterminous United States (CONUS) in this paper].

increased to have nine levels instead of six to improve the diurnal cycle near the surface. These enhancements to RUC LSM (Table 1), along with test results from stand-alone, one-dimensional experiments, and within the coupled RAP framework, are described in section 2. All of these enhancements are available in WRF using the RUC LSM option. Section 3 describes the new Moderate Resolution Imaging Spectroradiometer (MODIS)-derived classification of land surface properties available in WRF and used in the RAP and HRRR, providing more up-to-date land surface cover over its predecessor, the USGS land-use classification scheme used in the RUC. The improved RUC LSM also utilizes higher-resolution MODIS fractional photosynthetically active radiation (FPAR) and leaf area index (LAI) datasets to specify vegetation fraction and leaf area index (applied in RAP and HRRR). Section 3 also describes the new capability of the RUC LSM to specify land surface parameters as area-weighted averages in the grid box. Concluding remarks are presented in section 4.

## 2. Description of sea ice parameterization and modifications to the snow model

The RUC LSM contains heat and moisture transfer equations, together with energy and moisture budget equations for the ground surface, and uses an implicit

scheme for computing the surface fluxes (Smirnova et al. 1997). The energy and moisture budgets are applied to a thin layer spanning the ground surface and consider the heat capacities and densities of both the soil/snow and the atmosphere. The version of this model, tested in 1D offline tests and implemented in the first version of the RAP model, had six prognostic soil levels, ranging from the soil surface to 300 cm in depth (0, 5, 20, 40, 160, and 300 cm). The version in the WRF repository (version 3.4.1 since 2012; Table 1) used in the operational RAPv2 (Benjamin et al. 2016) uses nine prognostic soil levels (0, 1, 4, 10, 30, 60, 100, 160, and 300 cm), with highest vertical resolution near the surface (top layer of 1 cm). The thinner top soil layer with nine levels provides a stronger diurnal cycle as shown in a parallel RAP experiment (Fig. 2). The smaller cold bias in daytime and warm bias at nighttime results from use of the nine-level LSM compared to that with the six-level LSM. The RUC LSM has a snow model with one or two additional snow levels depending on snow depth and a simple parameterization of the processes in frozen soil (Smirnova et al. 2000). Recent enhancements to the RUC LSM in all of these areas are addressed below and summarized in Table 1.

### a. Parameterization of processes in sea ice

Treatment of processes in sea ice has been added to the RUC LSM parameterizations. This was deemed

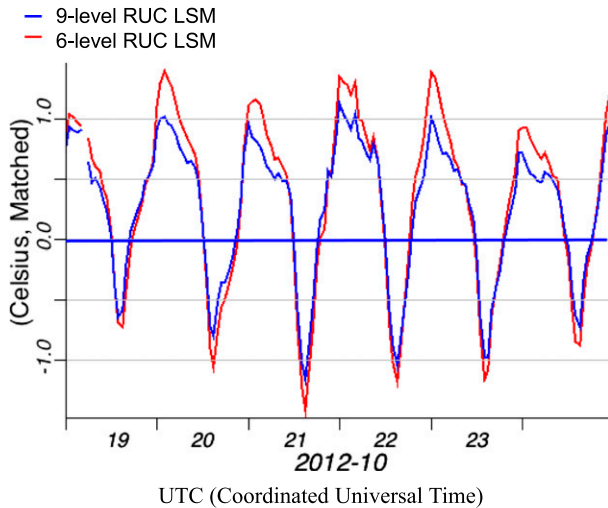


FIG. 2. The 2-m temperature bias (forecast – observations) from the RAP 12-h forecasts using 6-level (red) and 9-level (blue) versions of the RUC LSM over the entire RUC domain (Fig. 1).

necessary due to RAP domain coverage in high-latitude ocean areas. The ice model accounts for thermodynamic processes by solving the vertical heat diffusion equation:

$$\frac{\partial T_i}{\partial t} = \frac{\partial}{\partial z} \left( \frac{\nu_i}{\rho_i c_i} \frac{\partial T_i}{\partial z} \right), \quad (1)$$

where  $T_i$  is the temperature, and  $\nu_i$ ,  $c_i$ , and  $\rho_i$  are sea ice thermal conductivity, specific heat capacity, and density, respectively (a list of symbols is provided in the appendix). Sea ice properties are assumed to be those of pure ice. To limit computational expense for short-range weather prediction applications, the adjustment for ice salinity is disregarded for now. This parameterization is applied equally to sea ice and lake ice. The specific heat capacity for pure ice is computed from an empirical formula for temperatures from  $-2^\circ$  to  $-40^\circ\text{C}$  (Zubov 1963):

$$c_i = 0.5057 + 0.001863T_i, \quad (2)$$

where  $T_i$  is the temperature ( $^\circ\text{C}$ ). The coefficient of thermal conductivity of pure ice devoid of air bubbles is set to

$$\nu_i = 2.260872 \text{ J}(\text{m s K})^{-1}, \quad (3)$$

based on an average of published values. The density of pure ice is given by

$$\rho_i = \frac{\rho_0}{1 + 0.000165T_i}, \quad (4)$$

where  $\rho_0$  is pure ice density at  $0^\circ\text{C}$  ( $917.6 \text{ kg m}^{-3}$ ).

The energy budget at the sea ice surface is written as

$$\begin{aligned} & (\rho_a c_p \Delta z_a + \rho_i c_i \Delta z_i) \frac{\partial T_{\text{sk}}}{\partial t} \\ & = (R_n - H - L_s E - M_i) \Big|_{\Delta z_a} - G_i \Big|_{\Delta z_i}, \end{aligned} \quad (5)$$

where  $\Delta z_a$  is the height of the middle of the first atmospheric layer,  $\Delta z_i$  is the depth of the middle of the top layer of sea ice,  $T_{\text{sk}}$  is the mean temperature of a thin layer spanning the atmosphere–ice interface,  $R_n$  is the net radiative flux into the surface layer,  $H$  is the sensible heat flux into the atmosphere,  $L_s$  is the latent heat of sublimation,  $E$  is the sublimation rate, and  $G_i$  is the heat flux into the sea ice. With  $T_{\text{sk}}$  constrained to stay below the sea ice freezing point, the energy budget may produce a positive residual  $M_i$  that could be used to melt sea ice. However, currently the RUC LSM does not provide treatment of melted sea ice. Sea ice coverage in RAP is updated daily from the operational IMS (Interactive Multisensor Snow and Ice Mapping System) Northern Hemisphere Snow and Ice Analysis at 4-km resolution (Helfrich et al. 2007).

When snow falls on a sea ice surface, a two-layer snow model is applied to the snow accumulated on sea ice in a manner similar to snow accumulation on land (Smirnova et al. 2000). In this case, the energy budget equation is applied to the atmosphere–snow interface:

$$\begin{aligned} & (\rho_a c_p \Delta z_a + \rho_{\text{sn}} c_{\text{sn}} \Delta z_{\text{sn}}) \frac{\partial T_{\text{sk}}}{\partial t} \\ & = (R_n - H - L_s E - M_{\text{sn}}) \Big|_{\Delta z_a} - G_{\text{sn}} \Big|_{\Delta z_{\text{sn}}}, \end{aligned} \quad (6)$$

where  $M_{\text{sn}}$  is an energy budget residual when snow-surface temperature is constrained not to exceed the freezing point, and this residual energy is used to melt snow. Application of the snow model in areas covered with sea ice has been found to be helpful in producing realistic surface conditions, aided further by the hourly cycling of snow depths and snow temperatures in the RAP. This cycling of LSM conditions, including snow, allows the RAP (or HRRR) to maintain physically realistic vertical air–surface temperature differences (either positive or negative or near zero) at each grid point. In the simplified approach previously used in the RUC LSM, snow did not accumulate on the sea ice surface and sea ice skin temperature was equated to that at the first atmospheric level. Now, the solution of the energy budget in (6) takes into account the insulating effects of the snow cover and may produce warmer skin temperatures in snow-covered sea ice regions during the daytime. This is demonstrated in a case study comparison (Fig. 3a, off the northern coast of Alaska), and also in



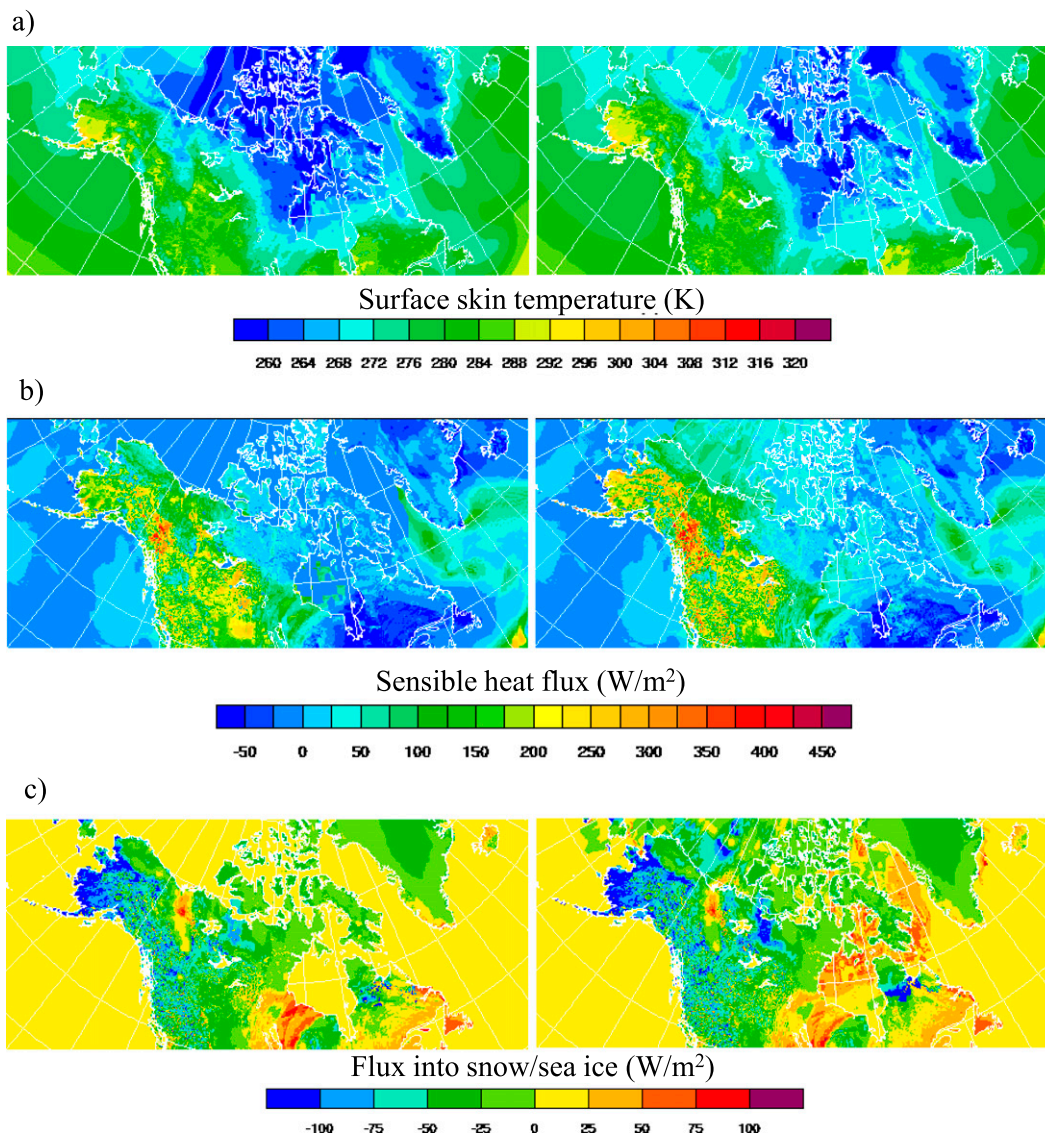


FIG. 3. Comparison of Rapid Refresh 12-h forecasts, valid at 0000 UTC 14 May 2009, of (a) skin temperature, (b) sensible heat flux, and (c) flux into snow/sea ice in the Arctic region of RAP, for the RUC LSM (left) without and (right) with sea ice parameterization.

warmer surface-layer temperatures from the positive upward sensible heat fluxes (Fig. 3b). The case study presented in Fig. 3 demonstrates that during the day positive downward heat fluxes from the surface of sea ice into its deeper layers (Fig. 3c) store heat inside sea ice, precluding the unrealistically cold nighttime 2-m temperatures resulting from the previous approach in this case.

This more sophisticated sea ice treatment has been important for Arctic applications in the WRF Rapid Refresh. For example, weather predictions over land in such regions as Alaska can be significantly improved from more realistic surface conditions, where nearby sea

ice may be present in adjacent waters for much of the year. Figure 4a presents an example of a common synoptic situation for the Alaska region, where onshore winds bring air inland from the nearby ice-covered Bristol Bay. With the previous approach without RAP-cycled snow temperatures on sea ice, unrealistically cold temperatures over sea ice led to significant 2-m cold biases over inland regions of Alaska (circled region, Fig. 4b). With the new treatment of snow on sea ice in the RUC LSM, warmer near-surface layers over sea ice were produced and transported inland, significantly reducing RAP inland cold biases in southwestern Alaska for this case (circled region, Fig. 4c).

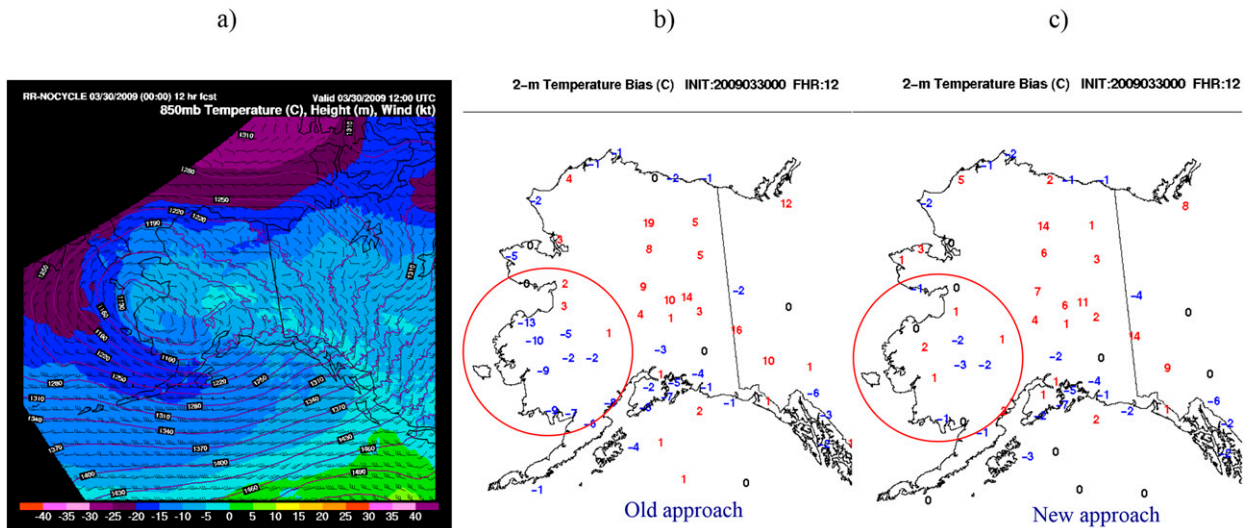


FIG. 4. (a) RAP 12-h forecast over Alaska for 850-hPa temperature (colors, °C), height (contours, m), and wind barbs (knots; 1 kt = 0.51 m s<sup>-1</sup>). Also 2-m temperature errors (°C, forecast - observation, red for + and blue for -) with (b) old and (c) new treatment of sea ice. Circled regions are affected by the air mass formed over sea ice. Valid time 1200 UTC 30 Mar 2009.

## b. Modifications to the RUC LSM snow model

### 1) SNOW MELTING ALGORITHM

Previous monitoring of RUC LSM behavior during the cold season revealed weaknesses in its snow model. Excessive snow melting rates associated with warm advection over snow were one such deficiency. During these events, sensible heat fluxes from the warm atmosphere toward the cold snow surface could become very large. As a result, energy budget residuals [Eq. (6), term  $M_{sn}$ ] used for snowmelt could also become very large, causing large amounts of snowmelt during a single time step. However, field experiments have demonstrated that melting rates are physically limited and depend on vertical temperature gradients just above the surface (Eggleston et al. 1971). When energy residuals from the model energy budget solution exceed a maximum threshold for realistic snowmelt, the excess energy can be assumed to warm the air nearest the snow surface. As a result, skin temperatures can rise to above freezing, even with snow on the ground. The 2-m air temperature can also warm, but with a corresponding reduction in snow melting rates and an overall prolonged presence of snowpack.

This strategy of limiting melting rates has now been implemented in the RUC LSM via a two-iteration solution of the energy budget [Eq. (6)]. At the first iteration, the skin temperature is limited to 273.15 K (with the full snow coverage of the grid cell), and the residual energy [Eq. (6), term  $M_{sn}$ ] is computed. After constraints on melting rates for given conditions (Eggleston

et al. 1971) are applied, an updated maximum possible energy for snowmelt is determined. If this updated  $M_{sn}$  is less than that from the first iteration, the updated  $M_{sn}$  is retained in the overall solution, providing more realistic (slower) snow melting rates and warmer (above freezing) skin temperatures.

Offline testing of modified snowmelt physics in the RUC LSM using SnowMIP2 data over multiple years and for different locations confirmed that the two-iteration algorithm helps to produce more realistic snow melting rates in spring season. The new algorithm was also tested in the coupled model (RAP) in winter for a 10-day period, 1–10 January 2015. This period featured several snow storms passing through the U.S. southern plains, Midwest, and North Atlantic states. One particular snow storm over Arizona, New Mexico, and Texas on 2–3 January 2015, with rapid snowmelt expedited by warm advection from nearby snow-free areas, provided a good case to see the benefits from changes to the snow melting algorithm. As anticipated, the control run with the old approach was melting snow too fast, causing underestimation of its snow cover on the next day after the passage of the snowstorm. Deficient snow cover in the control run on 4 January 2015 contributed toward its larger warm biases (Fig. 5a) and higher 2-m temperature RMS errors (Fig. 5b) averaged over the entire continental U.S. (CONUS) domain compared to the test run with the new two-iteration algorithm. Other days of the 10-day period featured slow melting processes and did not show any significant differences between the two runs. Also, excessive melting in the control run was mitigated by using IMS snow-sea

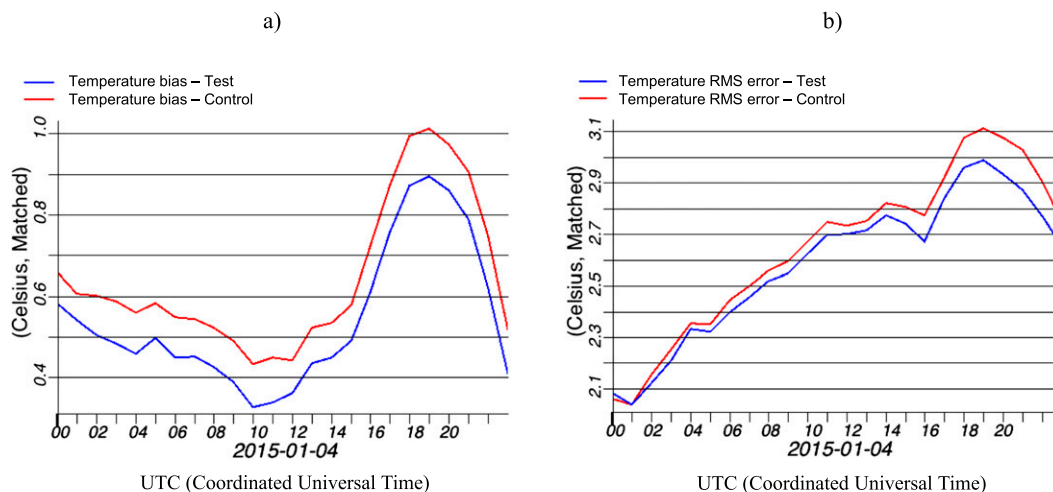


FIG. 5. RAP forecast error vs METAR surface observations. (a) Biases (forecast – observation) and (b) RMS errors for 12-h forecasts of 2-m temperature averaged over the CONUS domain (Fig. 1) for 1–10 Jan 2015. Control run (red line) uses old snow melting algorithm; test run (blue line) utilizes two-iteration snow melting approach.

ice data (Helfrich et al. 2007) to update the horizontal snow coverage once daily.

The snow updating procedure (Benjamin et al. 2016, their section 4) conducted once daily at 0000 UTC includes trimming of horizontal model snow coverage if there is no snow in the IMS snow/sea ice data for the given grid point and only if there is no snow precipitation in the model. The algorithm keeps track of trimmed snow water equivalent and adds it to existing neighboring points with missing snow compensating for possible shifts in model snow precipitation placement. For grid points with missing snow that do not have neighbors with trimmed snow, the value of built snow water equivalent is computed as an average from the neighboring snow points or, in case this is a standalone grid point with missing snow, is set to a minimum value of  $1 \text{ kg m}^{-2}$ . A similar procedure is used to decrease skin and soil temperatures (three levels in soil with a six-level configuration and five levels with a nine-level configuration) if they exceed 273 K for the points with built snow.

While both runs applied the daily snow-updating procedure, the control run received larger benefits from the snow-building component that helped to correct significant underestimation of cycled snow in this run. When the snow-updating procedure was applied at 0000 UTC 4 January, the number of points with built snow was 26% higher in the control run, and the overall number of grid points with corrected snow cover was 8% higher. This indicates that the two-iteration snow-melting algorithm produced more realistic melting rates and more accurate snow cover on the ground. Both RAP runs (Figs. 6a,b) were compared to the National Operational

Hydrologic Remote Sensing Center (NOHRSC) daily snow analyses valid at 0600 UTC (Fig. 6c). This comparison shows that even after snow updating, the control run still has underestimated snow-water equivalent values and less accurate location of the snowband across Arizona, New Mexico, and Texas (Fig. 6a; see area inside the red oval) than the experimental run (Fig. 6b). In the next snow update on 5 January 2015, the number of points with built snow in the control run was 33% higher, meaning that excessive melting rates in this run persisted. This example illustrates that both snow updating from the IMS snow product and improvements in the snow-melting algorithm contribute to a correct coverage of cycled snow in RAP.

## 2) SNOW ALBEDO

Further efforts were undertaken to achieve a more accurate representation of snow-surface properties, such as albedo, that strongly influence the energy budget. As a first step, a climatological, area-weighted, clear-sky maximum surface albedo in snow-covered areas, computed from Defense Meteorological Satellite Program (DMSP) imagery brightness in  $1^\circ$  latitude–longitude cells (Robinson and Kukla 1985), has been included in the RAP version of the RUC LSM. This dataset, available in WRF, depicts highest values of surface albedo ( $\sim 0.80$ ) in snow-covered high-latitude tundra and open shrubland regions, minimum values ( $\sim 0.35$ ) within the  $56^\circ$ – $60^\circ\text{N}$  zonal region, where snow albedo is affected by the prevalent boreal forest cover, and more typical values for snow albedo ( $\sim 0.70$ ) over the U.S. Great Plains, where crop and grassland vegetation types are dominant (Fig. 7). These values of surface albedo are interpolated to the RAP grid and



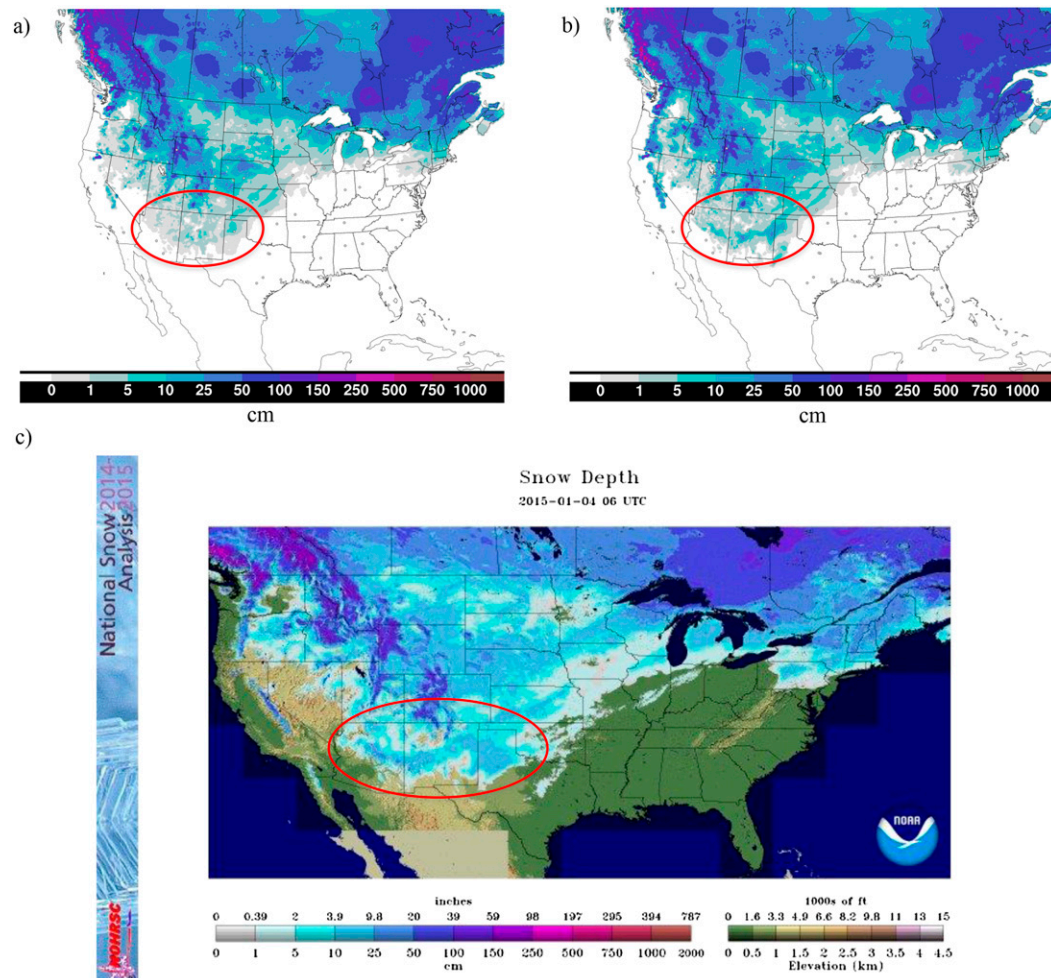


FIG. 6. Cycled RAP snow depth over the CONUS domain valid at 0600 UTC 4 Jan 2015 from (a) the control run with the old snow melting algorithm and (b) the test run with the two-iteration snow-melting approach. (c) Snow depth from the NOHRSC snow analyses valid at 0600 UTC 4 Jan 2015. Red oval indicates the area with improved snow cover from the new snow melting approach.

provide vegetation-dependent spatial variability in the surface albedo in areas of snow cover instead of the constant value of snow albedo (0.75) used previously.

Several modeling studies have found that use of this dataset can have a large impact on the surface energy budget and near-surface temperatures (e.g., Viterbo and Betts 1999), affecting the timing of spring snowmelt and subsequent streamflow peaks (Thomas and Rowntree 1992). Similar impacts were monitored in the RAP application, especially pronounced in snow-covered forested regions of Canada, Alaska, and the eastern part of the continental U.S. domain with lower values of maximum surface albedo (Fig. 7).

The RAP control simulation with constant value of fresh snow albedo equal to 0.75 and experimental simulation with the use of this maximum surface albedo

dataset were performed for the same 10-day period in January 2015 as described in section 2b(1). During and after passages of several snowstorms, more accurate specification of surface albedo in the experimental configuration showed improved performance near the surface. In particular, daytime cold biases in 6-h forecasts of 2-m temperature averaged over the eastern U.S. region were smaller in the experimental simulation due to increased amount of solar energy absorbed by the surface layer (Fig. 8a). Also, average 2-m temperature STD errors were reduced during the day, while at night, when surface albedo has no influence on model performance, errors remain at the same level (Fig. 8b). Figure 8 demonstrates that daytime improvements in surface temperature predictions from better representation of surface albedo, and consequently a more accurate surface energy budget, can



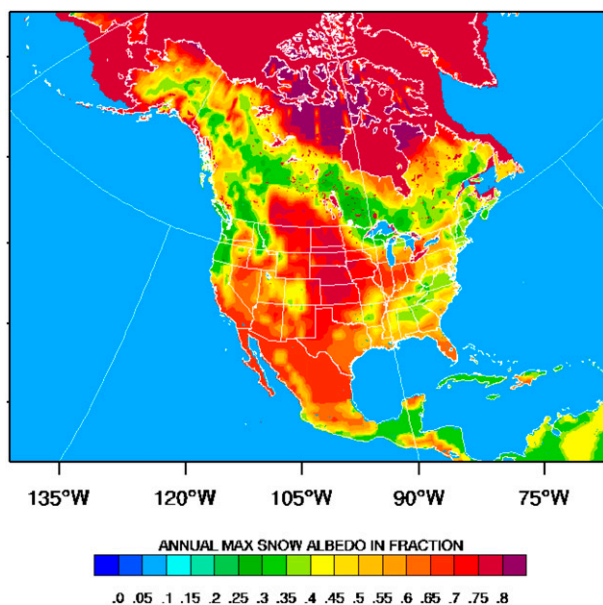


FIG. 7. Maximum surface albedo of snow-covered land measured from DMSP imagery in  $1^\circ \times 1^\circ$  latitude–longitude cells (Robinson and Kukla 1985) for the 13-km RAP domain.

be substantial. Therefore, to further improve near-surface predictions in snow-covered regions of RAP and HRRR, our future plans include testing a recently developed higher-resolution  $0.05^\circ$  dataset of maximum surface albedo of the snow-covered land generated from several MODIS sensors (Barlage et al. 2005).

In addition to its dependence on vegetation type, snow albedo in the RUC LSM (as implemented in RAP)

varies as a function of snow age, snow depth, and also snow temperature (when it approaches the melting point of  $0^\circ\text{C}$ ). The temperature dependence of snow albedo is such that higher temperatures lower the albedo due to meltwater pockets on the surface and changes to the ice crystal structure (Robock 1980; Petzold 1977). Following Robock (1980), snow and ice albedos are assumed to vary linearly from a maximum surface value for a snow-covered area at  $T \leq -10^\circ\text{C}$  to a “meltwater” value at  $T \geq 0^\circ\text{C}$ , where the meltwater value equals 0.4 for flat surfaces (cropland, grassland, sea ice, etc.) and 0.3 for forests.

The temperature dependence of RUC LSM snow albedo was tested offline using observed atmospheric conditions from SnowMIP2 over multiple years and for several grassland and forest locations in Canada, the United States, and Europe (Essery et al. 2009; Rutter et al. 2009). Figure 9a (<http://xweb.geos.ed.ac.uk/~ressery/SnowMIP2/results.html>) shows, as an example, snow-water equivalent simulations at a grassland location in the Swiss Alps from all LSMs participating in SnowMIP2 for the 2003/04 winter season. The spread among the models is substantial, especially during the snow melting season. Many models melted snow too rapidly, whereas others were too slow, including the RUC LSM. The standalone result from the RUC LSM for the same location demonstrates that the RUC LSM captures well the observed variations of snow cover on the ground during the first half of the winter season (Fig. 9b, red curve). But in spring, the RUC LSM is among the models that maintain snowpack for too long. The

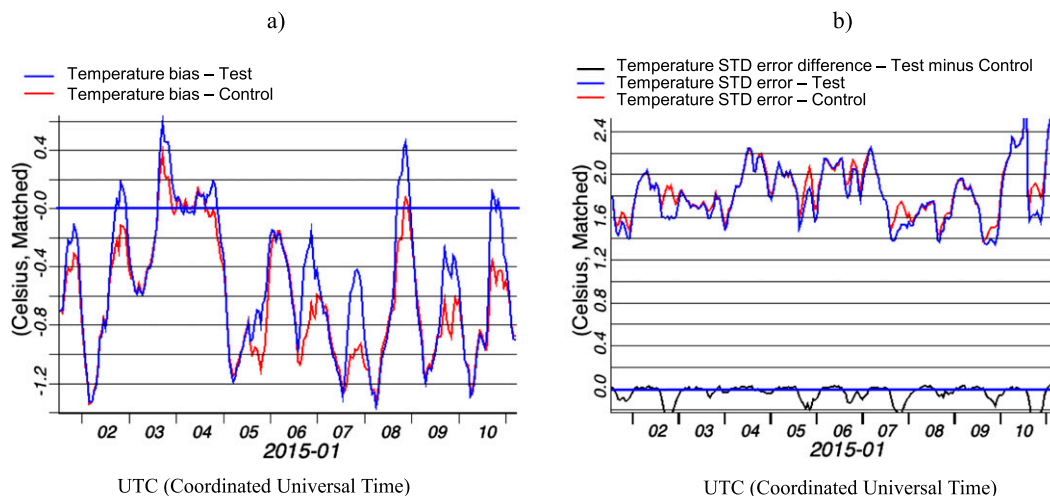


FIG. 8. RAP 6-h forecast error of 2-m temperature vs METAR surface observations. (a) Biases (forecast – observation) and (b) STD errors averaged over the eastern part of the CONUS domain (Fig. 1) for 1–10 Jan 2015. Control run (red line) uses constant value of fresh snow albedo equal to 0.75; test run (blue line) utilizes clear-sky maximum surface albedo of snow-covered land, computed from DMSP imagery brightness in  $1^\circ$  latitude–longitude cells (Robinson and Kukla 1985); test minus control (black line).

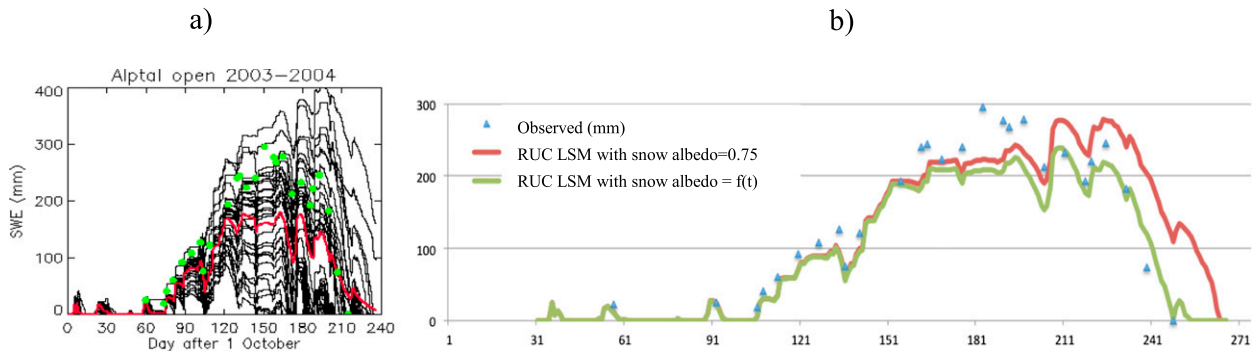


FIG. 9. Snow-water equivalent during the winter season of 2003/04 at a grassland location in Alptal, Switzerland ( $47^{\circ}\text{N}$ ,  $8^{\circ}\text{E}$ , elevation 1220 m), (data provided by Swiss Federal Institute for Forest, Snow and Landscape Research WSL): (a) simulation from all 27 models participating in SnowMIP2 experiment (red = average over 27 models, large green dots = observed) and (b) snow-water equivalent observed (blue triangles) and from the RUC LSM with the constant snow albedo = 0.75 (red curve) and with albedo dependent on surface temperature (green curve).

constant snow albedo (0.75) previously used in the RUC LSM is the primary reason for this snowpack maintenance, a value too high for the spring melting season. Implementing the albedo temperature dependence described previously has helped to achieve a more realistic solution of surface energy budget during the springtime, while not degrading model performance at other times (Fig. 9b, green curve).

After extensive offline testing in SnowMIP2, this snow albedo refinement was implemented in the coupled Rapid Refresh. An example for a spring day with active snow melting in the Arctic (Fig. 10) shows that with this new approach, the portion of the domain covered by snow or ice exhibits albedos ranging from 0.5 to 0.8 (Fig. 10b), compared to the constant albedo values of 0.55 for sea ice and 0.75 for snow (Fig. 10a) with the old approach. Based on offline testing, reduced albedos near the melting point can also produce more realistic snow

melting rates in the coupled RAP. The pattern of spatial variability also varies with time following the diurnal cycle of snow and sea ice temperature. Together with the new treatment of sea ice and snow cover and temperature cycling in RAP (see section 2a, above), spatial and temporal variabilities of snow albedo in the Arctic have the potential to improve estimated net radiation and available melting energy for better prediction of surface conditions in this area.

### 3. Switch to MODIS land-use classification and FPAR–LAI data to specify surface parameters in Rapid Refresh

Surface parameters such as aerodynamic-roughness length, leaf area index, and emissivity are specified based on the dominant vegetation category for the model grid box, as gridded by the WRF Preprocessing

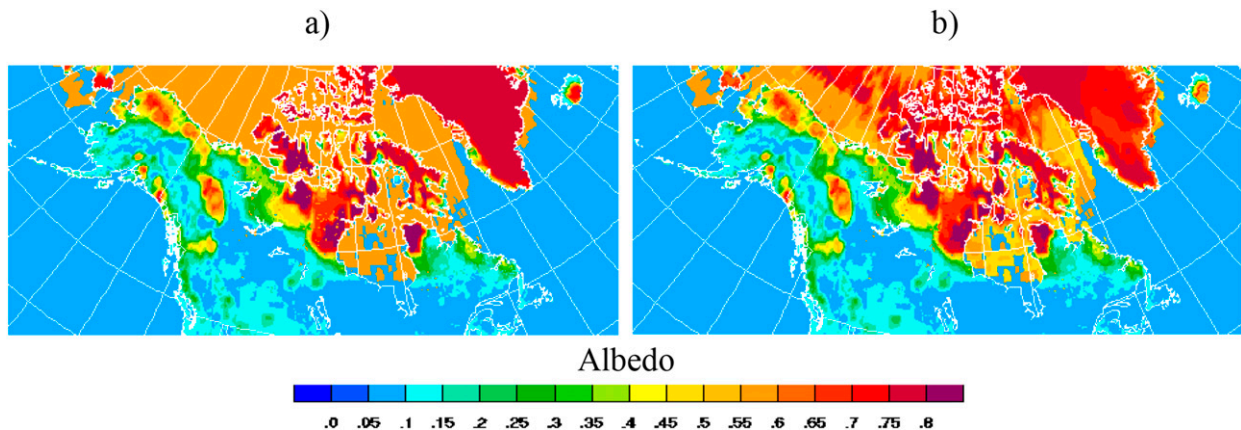


FIG. 10. Snow–ice albedo in the Arctic region of Rapid Refresh domain (Lambert conformal projection) for 13 May 2009: (a) before and (b) after implementation of snow–ice albedo temperature dependence.

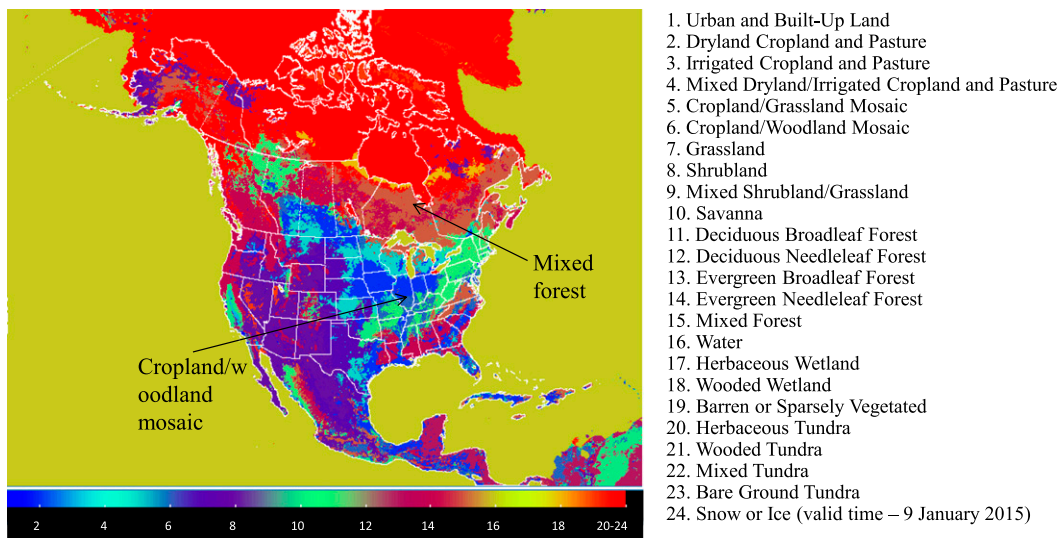


FIG. 11. USGS dominant land-use categories for Rapid Refresh domain.

System (WPS). WPS extracts the dominant land-use category and fractional land-use data on specific model grids from a global dataset with 30" horizontal resolution. By default, the WPS program uses AVHRR-based USGS data, and these data were also utilized during the early stages of RAP model development and in the first version of the operational RAP at NCEP. However, later an alternative dataset was added to WPS options, based on the MODIS land-cover classification of the International Geosphere–Biosphere Programme, and modified for the Noah land surface model (Wang et al. 2014). Several studies have demonstrated improved spatial and spectral characteristics in the MODIS data

compared to older AVHRR data (Hansen et al. 2000, 2002a,b). This suggests that the MODIS-derived vegetation maps more accurately represent the global land-cover distribution, and could be well suited for use in RAP.

The MODIS-based dataset contains 20 categories of land use, which are not a subset of the 24 USGS categories (cf. Figs. 11 and 12). Therefore, additional tables specifying surface parameters for the MODIS classification were provided for the RUC LSM starting with version 3.3 (released in 2011) of the WRF model. In addition to the new MODIS land-use classification, alternative datasets were added to WPS to specify vegetation fraction and leaf area index from 1-km resolution MODIS fractional

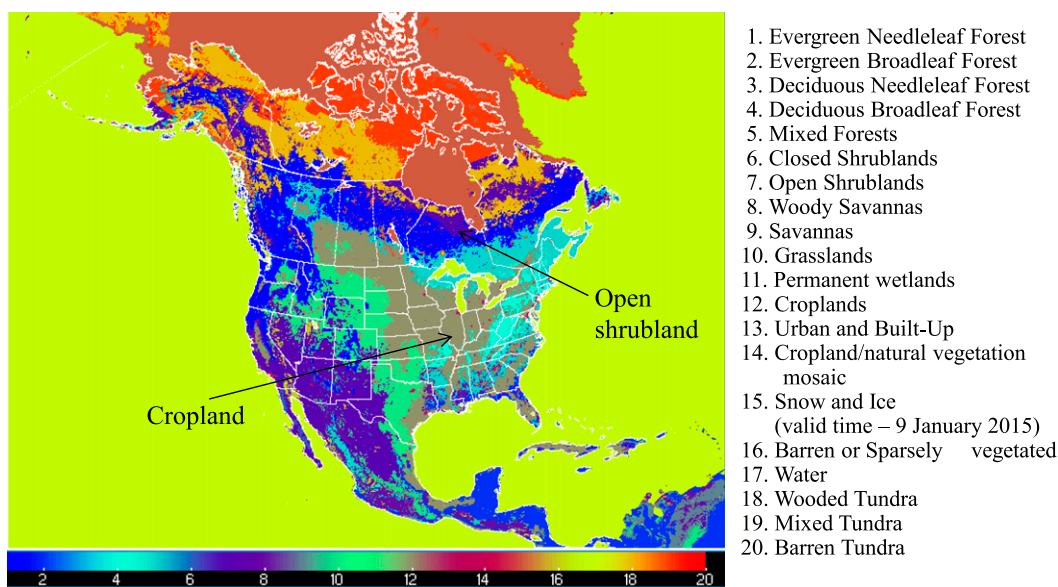


FIG. 12. MODIS dominant land-use categories for Rapid Refresh domain.



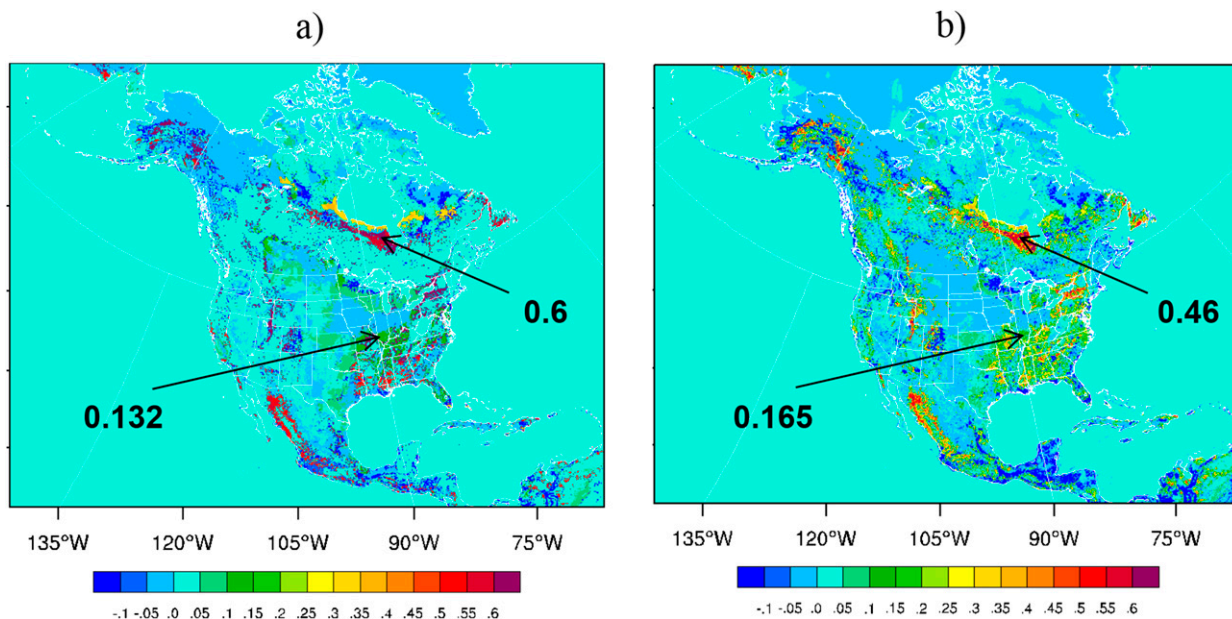


FIG. 13. Roughness length specified from USGS land-use classification minus roughness length from MODIS classification (a) with the use of dominant category approach and (b) with subgrid heterogeneity taken into account. Black numbers plotted on the figures indicate roughness lengths in meters.

photosynthetically active radiation and leaf area index datasets (Tian et al. 2000). These new datasets were also introduced into the second operational version of RAP.

Differences between the two classifications in several regions of the RAP domain can lead to substantial differences in such important land surface parameters as roughness length (Fig. 13a). For example, inland from the western coast of Hudson Bay use of open shrubland in MODIS (Fig. 12) instead of mixed forest in USGS (Fig. 11) reduces the roughness length by as much as 0.6 m (Fig. 13a). Similarly, use of the cropland category in MODIS (Fig. 12) instead of the cropland/woodland mosaic in USGS (Fig. 11) for the midwestern United States reduces roughness length by 0.132 m (Fig. 13a). Other regions of the RAP domain may have slightly higher or even slightly lower values of roughness length with the MODIS classification. Changes in this parameter certainly affect local wind speeds in the surface layer and the overall structure of the boundary layer. However, the overall statistical verification of surface variables for the RAP model has not been strongly affected by the transition to the MODIS land-use classification, implemented in RAPv2 (Benjamin et al. 2016).

A pronounced improvement in RAP low-level wind forecast skill was achieved by considering vegetation-based subgrid heterogeneity (Fig. 14). This method subdivides the surface within a RAP model grid box into several categories using MODIS or USGS land-use information. The effective values of surface parameters

are then computed as weighted averages of parameters from each of the represented categories. With this approach, surface characteristics exhibit smoother transitions between grid points with different dominant land-use categories, and also reflect local variabilities within the grid cell. Including subgrid heterogeneity also tends to reduce differences in surface roughness between the USGS and MODIS classifications (Fig. 13b), such that the switch to the MODIS classification appears to have less impact on surface predictions.

The capability of representing subgrid heterogeneity in RUC LSM was tested over a 10-day period in May 2013 in comparison to the control run of the model that used the dominant land-use category in each grid cell (Fig. 14). Both control and test configurations used WRF version 3.6 with the same suite of physics options including MYNN surface-layer and boundary layer schemes. The test version showed consistent improvement over the control configuration in the 12-h forecasts of 10-m wind for CONUS (Fig. 14), with mean positive wind speed biases reduction of about  $0.02 \text{ m s}^{-1}$  at night up to  $0.1 \text{ m s}^{-1}$  in daytime. Positive impacts from including subgrid heterogeneity on surface-wind predictions justified using this capability in the operational configuration of the RAP model.

#### 4. Conclusions

Enhancements to the RUC LSM since 2000, partly motivated by NOAA's transition from the RUC model



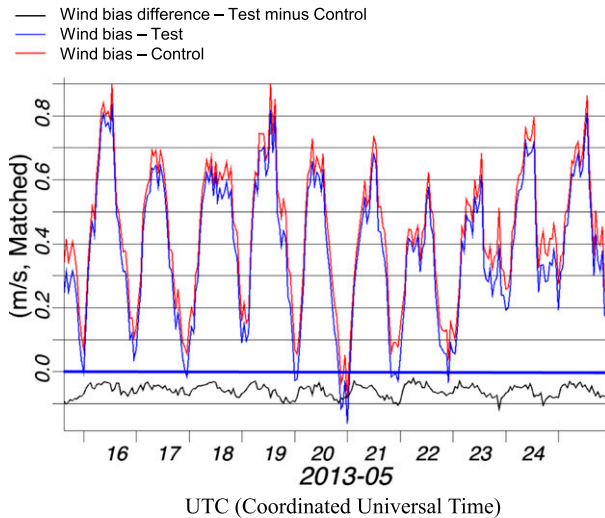


FIG. 14. RAP 10-m wind speed bias vs METAR observations for 12-h forecasts averaged over entire RUC domain (Fig. 1) for 16–25 May 2013 for the control run, which utilizes the dominant category approach (red), the test run, which takes into account subgrid heterogeneity (blue), and test minus control (black).

to the larger-domain RAP model, are summarized in Table 1. These enhancements focus on treatment for snow over land and ice and on the use of high-resolution MODIS land-use parameters. They have been tested within a stand-alone, one-dimensional framework and also coupled within the hourly-cycled RAP model, with improvement evident from individual components including in the Arctic region. Nevertheless, real-time RAP forecast performance metrics provide evidence that some RUC LSM parameterizations warrant further improvement. For example, the second version of the operational RAP (RAPv2) has revealed daytime warm or dry near-surface biases during the 2014 summer season, and cold 2-m temperature biases over snow during the 2014/15 cold season. Subsequent modifications in the RAP model physics suite, including RUC LSM, will become a part of the third version of operational RAP (RAPv3) at NCEP in 2016 (Benjamin et al. 2016).

Several very recent RUC LSM changes (not presented here) have been found to reduce the warm or dry bias in lower-tropospheric, daytime, warm-season RAP forecasts over land. These RUC LSM modifications are slated for inclusion in the next upgrade of the operational RAP. The modifications include tuning of several soil parameters to increase evapotranspiration, along with a simple representation of irrigation within cropland regions during the growing season. Including a seasonally varying roughness length over cropland, and MODIS-based leaf area index (LAI) climatology within deciduous vegetation, has also

contributed to improved RAP performance during the warm season.

In the cold season, further RUC LSM improvements could be achieved through implementing the mosaic approach for grid cells partially covered with snow. In this approach, the surface energy budget of the snow-covered and non-snow-covered portions of a grid cell are considered independently, and then these independently determined surface fluxes are aggregated to feed back into the surface-layer scheme. The benefits of the new approach will be assessed from the traditional methods of LSM evaluation referred to in the introduction and also from recently developed techniques for benchmarking intercomparisons (Best et al. 2015).

These very recent RUC LSM capabilities, along with the modifications detailed in this paper, have been made available in the version 3.7 (2015) release of the WRF model. Further work is in progress to make the RUC LSM available in the Land Information System (LIS) developed at NASA (Kumar et al. 2006). These recent (and continuing) improvements to the RUC land surface model improve its suitability for use within the WRF user community and for potential global applications. Inclusion of the RUC LSM within LIS will allow contributions to LIS applications within NASA and NOAA.

*Acknowledgments.* The work was supported by NOAA/ESRL and the Federal Aviation Administration (FAA) Weather Research Program. We thank John Osborn of NOAA/ESRL and two anonymous reviewers for thoughtful and very helpful reviews of the manuscript.

## APPENDIX

### List of Symbols

$c_i$ :	Sea ice specific heat capacity ( $\text{JK}^{-1}$ )
$c_{\text{sn}}$ :	Snow specific heat capacity ( $\text{JK}^{-1}$ )
$c_p$ :	Air specific heat capacity ( $\text{JK}^{-1}$ )
$E$ :	Sublimation rate ( $\text{kg m}^{-2} \text{s}^{-3}$ )
$G_i$ :	Heat flux into sea ice ( $\text{W m}^{-2}$ )
$G_{\text{sn}}$ :	Heat flux into snow ( $\text{W m}^{-2}$ )
$H$ :	Sensible heat flux ( $\text{W m}^{-2}$ )
$L_s$ :	Latent heat of sublimation ( $\text{J kg}^{-1}$ )
$M_i$ :	Energy budget residual spent on sea ice melt ( $\text{W m}^{-2}$ )
$M_{\text{sn}}$ :	Energy budget residual spent on snowmelt ( $\text{W m}^{-2}$ )
$R_n$ :	Net radiation flux ( $\text{W m}^{-2}$ )

$T_i$ :	Ice temperature (K)
$T_{sk}$ :	Temperature of atmosphere–surface interface (K)
$\nu_i$ :	Sea ice thermal conductivity ( $\text{W m}^{-1} \text{K}^{-1}$ )
$\rho_a$ :	Air density ( $\text{kg m}^{-3}$ )
$\rho_{sn}$ :	Snow density ( $\text{kg m}^{-3}$ )
$\rho_i$ :	Sea ice density ( $\text{kg m}^{-3}$ )
$\rho_0$ :	Sea ice density at $0^\circ\text{C}$ ( $\text{kg m}^{-3}$ )
$\Delta z_a$ :	Depth of atmospheric surface layer (m)
$\Delta z_i$ :	Depth of ice surface layer (m)
$\Delta z_{sn}$ :	Depth of snow surface layer

## REFERENCES

- Barlage, M., X. Zeng, H. Wei, and K. E. Mitchell, 2005: A global  $0.05^\circ$  maximum albedo dataset of snow-covered land based on MODIS observations. *Geophys. Res. Lett.*, **32**, L17405, doi:10.1029/2005GL022881.
- Benjamin, S. G., and Coauthors, 2004a: An hourly assimilation–forecast cycle: The RUC. *Mon. Wea. Rev.*, **132**, 495–518, doi:10.1175/1520-0493(2004)132<0495:AHACTR>2.0.CO;2.
- , G. A. Grell, J. M. Brown, T. G. Smirnova, and R. Bleck, 2004b: Mesoscale weather prediction with the RUC hybrid isentropic/terrain-following coordinate model. *Mon. Wea. Rev.*, **132**, 473–494, doi:10.1175/1520-0493(2004)132<0473:MWPWTR>2.0.CO;2.
- , and Coauthors, 2007: From the radar-enhanced RUC to the WRF-based Rapid Refresh. Preprints, *22nd Conf. on Weather Analysis and Forecasting/18th Conf. on Numerical Weather Prediction*, Park City, UT, Amer. Meteor. Soc., J3.4. [Available online at [https://ams.confex.com/ams/22WAF18NWP/techprogram/paper\\_124827.htm](https://ams.confex.com/ams/22WAF18NWP/techprogram/paper_124827.htm).]
- , and Coauthors, 2016: A North American hourly assimilation and model forecast cycle: The rapid refresh. *Mon. Wea. Rev.*, in press.
- Berbery, E. H., K. Mitchell, S. Benjamin, T. Smirnova, H. Ritchie, R. Hogue, and E. Radeva, 1999: Assessment of land-surface energy budgets from regional and global models. *J. Geophys. Res.*, **104**, 19 329–19 348, doi:10.1029/1999JD900128.
- Best, M. J., and Coauthors, 2015: The plumbing of land surface models: Benchmarking model performance. *J. Hydrometeorol.*, **16**, 1425–1442, doi:10.1175/JHM-D-14-0158.1.
- Eggleston, K. O., E. K. Israelsen, and J. P. Riley, 1971: Hybrid computer simulation of the accumulation and melt processes in a snowpack. Utah Water Research Laboratory, Paper 501, 77 pp. [Available online at [http://digitalcommons.usu.edu/water\\_rep/501/](http://digitalcommons.usu.edu/water_rep/501/).]
- Essery, R. L. H., and Coauthors, 2009: SnowMIP2: An evaluation of forest snow process simulations. *Bull. Amer. Meteor. Soc.*, **90**, 1120–1135, doi:10.1175/2009BAMS2629.1.
- Etchevers, P., and Coauthors, 2002: SnowMIP, an intercomparison of snow models: First results. *Proc. Int. Snow Science Workshop*, Penticton, BC, Canada, 353–360. [Available online at <http://arc.lib.montana.edu/snow-science/objects/issw-2002-353-360.pdf>.]
- , and Coauthors, 2004: Validation of the surface energy budget simulated by several snow models. *Ann. Glaciol.*, **38**, 150–158, doi:10.3189/172756404781814825.
- Hansen, M. C., R. S. DeFries, J. R. G. Townshend, and R. Sohlberg, 2000: Global land cover classification at 1 km spatial resolution using a classification tree approach. *Int. J. Remote Sens.*, **21**, 1331–1364, doi:10.1080/014311600210209.
- , —, —, L. Marufu, and R. Sohlberg, 2002a: Development of a MODIS tree cover validation data set for Western Province, Zambia. *Remote Sens. Environ.*, **83**, 320–335, doi:10.1016/S0034-4257(02)00080-9.
- , —, —, R. A. Sohlberg, C. Dimiceli, and M. Carroll, 2002b: Towards an operational MODIS continuous field of percent tree cover algorithm: Examples using AVHRR and MODIS data. *Remote Sens. Environ.*, **83**, 303–319, doi:10.1016/S0034-4257(02)00079-2.
- Helfrich, S. R., D. McNamara, B. H. Ramsay, T. Baldwin, and T. Kasheta, 2007: Enhancements to, and forthcoming developments in the Interactive Multisensor Snow and Ice Mapping System (IMS). *Hydrol. Processes*, **21**, 1576–1586, doi:10.1002/hyp.6720.
- Kumar, S. V., and Coauthors, 2006: Land Information System—An interoperable framework for high resolution land surface modeling. *Environ. Model. Softw.*, **21**, 1402–1415, doi:10.1016/j.envsoft.2005.07.004.
- Luo, L., and Coauthors, 2003: Effects of frozen soil on soil temperature, spring infiltration, and runoff: Results from the PILPS 2(d) experiment at Valdai, Russia. *J. Hydrometeorol.*, **4**, 334–351, doi:10.1175/1525-7541(2003)4<334:EOFSOS>2.0.CO;2.
- Petzold, R. E., 1977: An estimation technique for snow surface albedo. *Climatol. Bull.*, **21**, 1–11. [Available online at <http://www.cmosarchives.ca/CB/cb110101.pdf>.]
- Robinson, D. A., and G. Kukla, 1985: Maximum surface albedo of seasonally snow-covered lands in the Northern Hemisphere. *J. Climate Appl. Meteorol.*, **24**, 402–411, doi:10.1175/1520-0450(1985)024<0402:MSAOSS>2.0.CO;2.
- Robock, A., 1980: The seasonal cycle of snow cover, sea ice and surface albedo. *Mon. Wea. Rev.*, **108**, 267–285, doi:10.1175/1520-0493(1980)108<0267:TSCOSC>2.0.CO;2.
- Rutter, N., and Coauthors, 2009: Evaluation of forest snow processes models (SnowMIP2). *J. Geophys. Res.*, **114**, D06111, doi:10.1029/2008JD011063.
- Schlosser, C. A., A. Robock, K. Y. Vinnikov, N. A. Speranskaya, and Y. Xue, 1997: 18-year land surface hydrology model simulations for a midlatitude grassland catchment in Valdai, Russia. *Mon. Wea. Rev.*, **125**, 3279–3296, doi:10.1175/1520-0493(1997)125<3279:YLSHMS>2.0.CO;2.
- Skamarock, W., J. B. Klemp, J. Dudhia, D. O. Gill, D. Barker, M. G. Duda, X.-Y. Huang, and W. Wang, 2008: A description of the Advanced Research WRF version 3. NCAR Tech. Note NCAR/TN-475+STR, doi:10.5065/D68S4MVH.
- Slater, A. G., and Coauthors, 2001: The representation of snow in land surface schemes: Results from PILPS 2(d). *J. Hydrometeorol.*, **2**, 7–25, doi:10.1175/1525-7541(2001)002<0007:TROSIL>2.0.CO;2.
- Smirnova, T. G., J. M. Brown, and S. G. Benjamin, 1997: Performance of different soil model configurations in simulating ground surface temperature and surface fluxes. *Mon. Wea. Rev.*, **125**, 1870–1884, doi:10.1175/1520-0493(1997)125<1870:PODSMC>2.0.CO;2.
- , —, and D. Kim, 2000: Parameterization of cold-season processes in the MAPS land-surface scheme. *J. Geophys. Res.*, **105**, 4077–4086, doi:10.1029/1999JD901047.
- Smith, T. L., S. G. Benjamin, J. M. Brown, S. Weygandt, T. Smirnova, and B. Schwartz, 2008: Convection forecasts from the hourly updated, 3-km High Resolution Rapid Refresh (HRRR) Model. Preprints, *24th Conf. on Severe Local Storms*, Savannah, GA, Amer. Meteor. Soc., 11.1.

- [Available online at <https://ams.confex.com/ams/pdfpapers/142055.pdf>.]
- Thomas, G., and P. R. Rowntree, 1992: The boreal forests and climate. *Quart. J. Roy. Meteor. Soc.*, **118**, 469–497, doi:10.1002/qj.49711850505.
- Tian, Y., Y. Zhang, J. Knyazikhin, R. B. Myneni, J. Glassy, G. Dedieu, and S. W. Running, 2000: Prototyping of MODIS LAI and FPAR algorithm with LASUR and LANDSAT data. *IEEE Trans. Geosci. Remote Sens.*, **38**, 2387–2401, doi:10.1109/36.868894.
- Viterbo, P., and A. K. Betts, 1999: Impact on ECMWF forecasts of changes to the albedo of the boreal forests in the presence of snow. *J. Geophys. Res.*, **104**, 27 803–27 810, doi:10.1029/1998JD200076.
- Wang, W., and Coauthors, 2014: User's Guide for the Advanced Research WRF (ARW) Modeling System version 3.6. UCAR, 428 pp. [Available online at [http://www2.mmm.ucar.edu/wrf/users/docs/user\\_guide\\_V3/contents.html](http://www2.mmm.ucar.edu/wrf/users/docs/user_guide_V3/contents.html).]
- Zubov, N. N., 1963: *Arctic Ice*. U.S. Navy Electronics Laboratory, 510 pp.